

Platinum overlaid PdCuIr/C: an Improved Methanol Oxidation Electrocatalyst

Yanjiao Ma¹, Rongfang Wang^{1,3,*}, Hui Wang¹ and Shan Ji²

¹ Key Laboratory of Eco-Environment-Related Polymer Materials, Ministry of Education of China, Key Laboratory of Gansu Polymer Materials, College of Chemistry and Chemical Engineering, Northwest Normal University, Lanzhou 730070, China

² South African Institute for Advanced Materials Chemistry, University of the Western Cape, Cape Town 7535, South Africa

³ Guangdong Key Lab for Fuel Cell Technology, South China University of Technology, Guangzhou 510641, China

*E-mail: wrf38745779@126.com

Received: 31 July 2012 / Accepted: 9 September 2012 / Published: 1 May 2013

A platinum overlaid PdCuIr/C (Pt-PdIrCu/C) anodic catalyst for direct methanol fuel cell was prepared by a two-step reduction method. Transmission electron microscopy (TEM) and X-ray diffraction (XRD) results show that the metal nano-particles had a large surface area and even distribution. The Pt mass activity of the catalyst was about 6.6 times larger than that of a Pt/C catalyst and 1.2 times larger than that of a Pt-PdCu/C catalyst. The high electrocatalytic activities could be attributed to the synergistic effect between Pt and PdIrCu.

Keywords: Electrocatalysts; Methanol Electrooxidation; Fuel Cells; Core-shell Structure; Alloy

1. INTRODUCTION

Low-temperature fuel cells offer a promising energy source for near-future energy demands [1, 2]. Within the low-temperature fuel cell category, direct methanol fuel cells (DMFCs) stand out due to their high energy density, efficiency, low weight, compact cell assembly, easy handling and distribution [2-5]. However, the commercialization of DMFCs was hindered by the high cost and reliability issues of effective anode and cathode catalysts [6]. Pt is most widely used as catalysts in fuel cell, but it has relatively low methanol oxidation reaction (MOR) kinetics at the anode, is easily poisoned by CO, and is not stable in the acidic conditions. These factors reduce its active surface area, performance and lifetime, and limit its application [3, 5].

In recent years, Pt-decorated Ru-based and Pd-based alloy catalysts have been investigated due to their relatively low cost and enhanced catalytic activities for the methanol oxidation in DMFCs [7-11]. Guo *et al.* reported that Pt-on-Pd bimetallic nano-dendrites electrocatalysts had much higher electrocatalytic activity in methanol oxidation than platinum black and commercial Pt/C catalysts [12]. Chen *et al.* reported that the Pt-on-Ru catalyst with low-Pt-loading had a higher mass-specific current than the PtRu black catalyst under acid conditions [8]. Wang *et al.* reported that fine-tuning of the Pt and Pd ratios afforded Pt-on-Pd nano-dendrites with superior electrocatalytic activity compared to commercial Pt electrocatalysts [13]. In our previous works, it was found that Pt-decorated PdCu/C catalyst show a high methanol oxidation activity, in which low cost Cu was used as core in its core-shell structure [14]. The use of such transition metals show exciting prospects for producing cost effective catalysts and highlights the need for understanding structure-property relationships underlying their beneficial effects.

Ir and Ir oxide used in Pt-based catalysts for methanol oxidation at the anode and for oxygen reduction at the cathode has been reported to have similar effects to Ru. It is likely that OH groups can be stabilized at the metallic Ir surface, and in turn assist in the oxidation of CO or other adsorbed intermediates. Furthermore, with a relatively high oxidation potential (1.156 V, Ir³⁺/Ir), Ir has a high resistance to dissolution under fuel cell operating conditions. Currently, there are a few reports on PtIr-based alloys and Ir-decorated Pt-based electrocatalysts for the DMFCs. Holt-Hindle *et al.* reported that the nanoporous PtIr electrodes have extraordinarily high electroactive surface areas. The results showed that Ir can significantly improve the electrocatalytic activity of Pt in methanol oxidation and oxygen reduction reactions [15]. Lee *et al.* prepared Pt overlayers on various catalysts by a two-step method, which resulted in high catalyst activity due to competitive contribution of CO_{ad} oxidation activity and high Pt utilization rate. It was found that the Pt overlayer on Ir nanoparticles, compared to that on Au nanoparticles, exhibited much higher methanol oxidation activity due to smaller diameter of the Ir nanoparticle and the positive effect of Ir on CO_{ad} oxidation activity [16]. These reports confirm the positive role of Ir in Pt-based catalysts for methanol electrooxidation.

To our knowledge, the present study is the first to synthesize and evaluate Pt-decorated PdIrCu alloy catalysts for methanol oxidation. Ir modification was used to increase Pt-Pd activity. To achieve high catalytic performance and low loading of Pt, a carbon support Pt-PdCuIr/C catalyst was prepared by a two-step method. The structure of Pt-PdCuIr/C was examined by transmission electron microscopy (TEM), X-ray diffraction (XRD) and electrochemical characterization. Intriguingly, it was found that the deposition of Pt on the PdCuIr nanoparticles resulted in higher MOR activity than that of the Pt/C and Pt-PdCu/C catalysts.

2. EXPERIMENTAL

Pt-PdCuIr/C catalyst was prepared by a two-step method. In a typical process, PdIrCu/C catalyst with a nominal weight Pd:Cu:Ir ratio of 3:3:1 was prepared as follows: Palladium chloride (PdCl₂, 38 mg), copper chloride dihydrate (CuCl₂, 36 mg), H₂IrCl₆ (37 mg) and sodium citrate (120 mg) were dissolved in ethylene glycol (EG, 20 mL) and stirred for 0.5 h. Pretreated carbon black

Vulcan[®] XC72R (150 mg) was added to the mixture with stirring. The pH of the system was adjusted to ~10 by the dropwise addition of a KOH/EG (5 wt%) solution with vigorous stirring. The mixture was then heated at 160°C for 6 h, and the product was collected by filtration, washed 5 times with deionized water and dried in air at 60°C for 12 h.

The as-prepared PdCuIr/C powder was then mixed with H₂PtCl₆·6H₂O (Pt ~5 wt% in weight ratio) aqueous solutions and stirred for 4 h at 80°C. The resulting Pt-PdCuIr/C catalyst powder was collected by filtration, washed with deionized water to remove any remaining chloride anion, and then dried in air at 60°C for 12 h. Pt-PdCu/C was synthesized by the same above procedure but excluding H₂IrCl₆.

The catalysts were characterized by XRD on a Shimadzu XD-3A (Japan), using filtered Cu-K α radiation. All X-ray diffraction patterns were analyzed using Jade 7.5 of Material Data, Inc. (MDI); peak profiles of individual reflections were obtained by a nonlinear least-square fit of the Cu K α corrected data. TEM-measurements were carried out on a Tecnai G220 S-TWIN (FEI Company); the acceleration voltage was 200 kV. The energy-dispersive X-ray spectroscopy (EDX) analysis was performed in an analyzer associated with TEM.

Electrochemical measurements of the catalysts were carried out on an electrochemical work station (Auto Lab), using a three-electrode cell. The counter and reference electrode were a platinum wire and an Ag/AgCl (3 M KCl) electrode respectively. The working electrode was a 5-mm diameter glassy carbon disk. The thin-film electrodes were prepared using 5 mg of electrocatalyst dispersed ultrasonically in Nafion/ethanol (1 mL, 0.25% Nafion) for 15 min, of which 8 μ L was transferred onto the glassy carbon disk and then dried in air.

3. RESULTS AND DISCUSSION

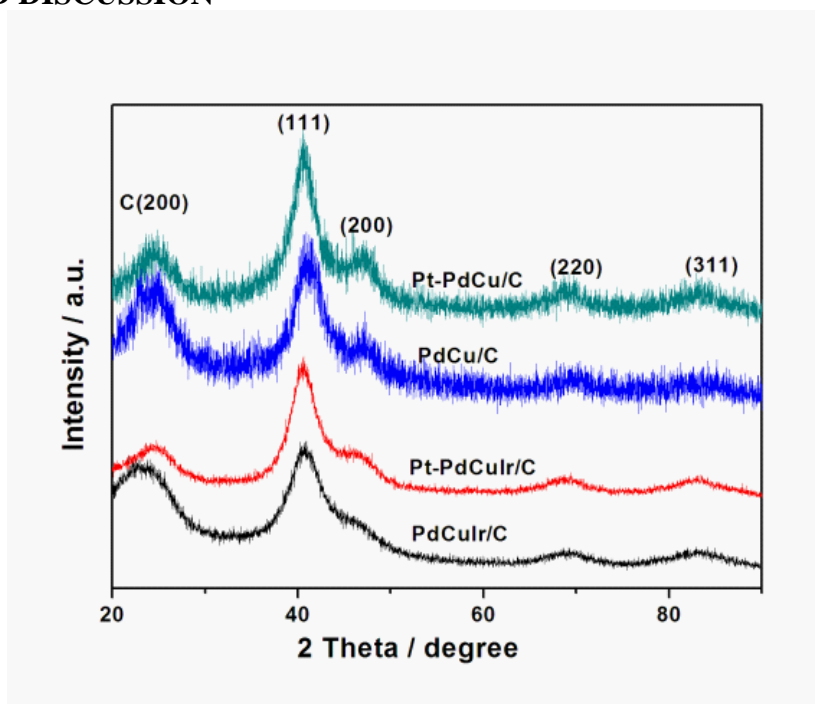


Figure 1. XRD patterns of PdCu/C, Pt-PdCu/C, PdCuIr/C, and Pt-PdCuIr/C catalysts.

XRD was used to determine the crystal structure of the PdCuIr/C, and Pt-PdCuIr/C catalysts. In our previous studies on bimetallic Pd-based nanoparticle (synthesized by the organic colloid method), it was found that the alloy particle sizes were in the range of 4-8 nm. After Ir was introduced into the system, the size of trimetallic particle was less than 3 nm. Fig.1 shows the XRD patterns of PdCuIr/C, Pt-PdCuIr/C with those of Pt-PdCu/C and PdCu/C for comparison. The first peak located at about 24.8° in all the XRD patterns is associated with the carbon support. The three characteristic peaks of face-centered cubic (fcc) crystalline Pt (Pd, PdCu or PdCuIr alloy), corresponding to the planes (1 1 1), (2 0 0), (2 2 0) and (3 1 1), were presented at 2θ values of ca. 40° , 47° , 68° , and 83° , respectively. The average particle size of PdCuIr/C, Pt-PdCuIr/C, PdCu/C and Pt-PdCu/C catalysts, which can be evaluated according to the Scherrer equation, were ca. 2.8, 3.1, 4.3 and 4.6nm, respectively. The (1 1 1) diffraction of Pt-PdCuIr/C and Pt-PdCu/C shifted slightly negatively compared to that of PdCuIr/C and PdCu/C, suggesting that some Cu, Ir and Pd atoms in the core had been displaced by the larger Pt atoms, leading to an expansion of lattice. The absence of Pt peaks implies that the size of the Pt nano-islands on the surface of PdCuIr and PdCu alloys was smaller than the detecting capability of XRD ($\sim 1\text{nm}$). That Pt atoms could deposit on PdCuIr nanoparticles can be attributed to: (i) the interaction between the Pt and PdCuIr metal alloy was stronger than that between Pt and carbon support; (ii) Pt and PdIrCu solid solution are all with face-centered cubic structure, which is in favor of the Pt growth on the PdCuIr alloy surface [17, 18].

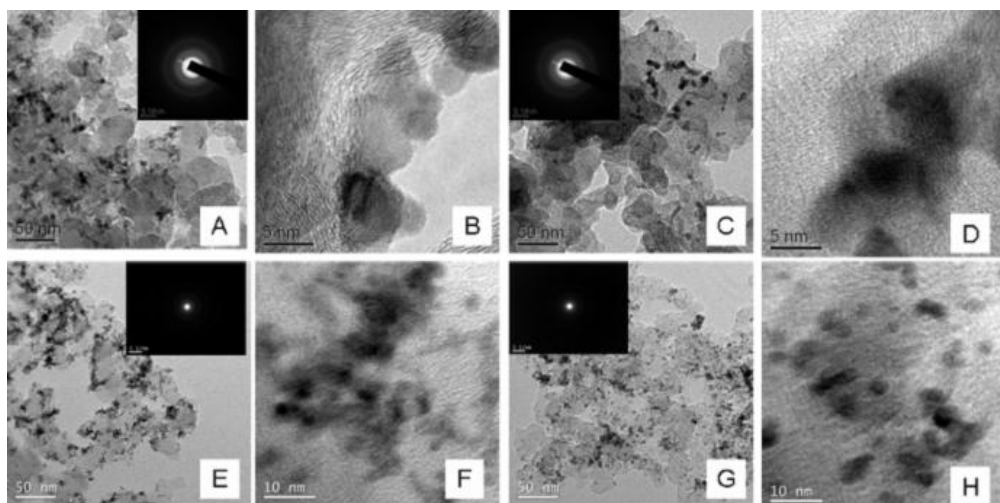


Figure 2. TEM images of PdCu/C, Pt-PdCu/C, PdCuIr/C, and Pt-PdCuIr/C catalysts; and HRTEM of PdCu/C, Pt-PdCu/C, PdCuIr/C, and Pt-PdCuIr/C catalysts. The inset in A, C, E, and G show the corresponding SAED patterns of PdCu/C, Pt-PdCu/C, PdCuIr/C, and Pt-PdCuIr/C catalysts.

Fig. 2 shows TEM images of PdCu/C (A), Pt-PdCu/C (C), PdCuIr/C (E) and Pt-PdCuIr/C (G). It was noted that the catalysts were highly dispersed on the carbon support with narrow size distribution. The carbon-supported alloy nanoparticles had spherical or elliptical shapes. One hundred particles were measured to obtain the particle size distribution. The average particle size of PdCu/C, Pt-PdCu/C, PdCuIr/C and Pt-PdCuIr/C catalysts was ca. 4.3, 4.5, 2.8 and 3.1 nm, respectively. No

obvious grain boundaries or defects were observed, as only a very small lattice mismatch existed between Pt and PdCu alloys.

The fine structures of the core and shell layers were further characterized using high resolution transmission electron microscopy (HRTEM). Fig. 2 also shows the HRTEM images of PdCu/C (B), Pt-PdCu/C (D), PdCuIr/C (F) and Pt-PdCuIr/C (H). An HRTEM study of a series of single nanoparticles shows that each nanoparticle had a polycrystalline structure. The measured distance between the two nearest atom rows for PdCu/C was 0.221 nm, i.e., less than the (111) interplanar distance of Pd (0.225 nm), indicative of a lattice contraction due to alloying. The HRTEM image of Pt-PdCu/C catalyst shows that the particle has an irregular polyhedral shape. The measured distance between the two nearest atom rows for Pt-PdCu/C is 0.232 nm. The HRTEM results suggest that in some cases discrete particles of Pt were formed rather than a complete layer. However, we couldn't observe the lattice of PdCuIr and Pt-PdCuIr in HRTEM images. This implies that PdCuIr/C and Pt-PdCuIr/C catalysts were in amorphous states. This was further illustrated by the selected area electron diffraction (SAED) patterns (see insets Fig. 2). The amorphous alloys and their modified electronic structure therefore may result in a better electrocatalytic activity [19-21].

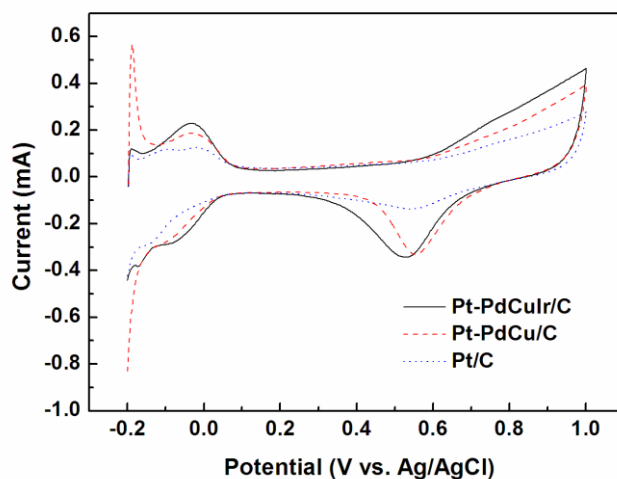


Figure 3. Cyclic voltammograms of Pt-PdCuIr/C, Pt-PdCu/C and Pt/C catalysts in 0.5 mol L⁻¹ H₂SO₄ solution at 50 mV s⁻¹ at room temperature

The structure of Pt decorated PdCuIr was also determined by cyclic voltammetry (CV), which can be used as a surface sensitive technique to detect the electrochemical properties of surface atoms rather than bulk atoms. Fig. 3 shows the CV plots of Pt-PdCu/C, Pt/C and Pt-PdCuIr/C electrodes in 0.5 M H₂SO₄ under N₂ atmosphere. Well defined chemical adsorption peaks of hydrogen on different Pt low-index surfaces became less definable for the Pt on PdCu and PdCuIr alloys. The electrochemical surface area of Pt particles is one of the most important parameters to determine the catalytic activity for MOR.

The real surface of Pt-based catalysts was estimated from the integrated charge of the hydrogen absorption region from the CV plot. The hydrogen absorption is significantly low in samples of PdCu/C possibly because of the alloying of Pd with Cu, indicating that the large Cu content inhibited

hydrogen absorption. Pt-PdCu/C also feature single absorption and desorption peaks that were noticeably different from hydrogen absorption and desorption from monometallic Pt/C and bimetallic PtRu/C. The difference is taken as an indication of the changes in the adsorption site geometry [22]. The electro-chemical active surface area (AEL) of different Pt-based catalysts was calculated according to Eq. (1) [14]:

$$A_{EL} (\text{m}^2 \text{g}^{-1}) = \frac{Q_H}{2.1 \times [\text{Pt}]} \quad (1)$$

where Q_H (C m^{-2}) is the charge exchanged during hydrogen desorption on the Pt surface, $[\text{Pt}]$ (g m^{-2}) is the Pt loading on the electrode, and 2.1 is the charge (C m^{-2}) required to oxidize a monolayer of hydrogen on the Pt surface. The A_{EL} are $35.9 \text{ m}^2 \text{g}^{-1}_{\text{metals}}$ for Pt/C, $59.1 \text{ m}^2 \text{g}^{-1}_{\text{metals}}$ for Pt-PdCu/C and $50.6 \text{ m}^2 \text{g}^{-1}_{\text{metals}}$ for Pt-PdCuIr/C, respectively. Based on the Pt mass, the specific A_{EL} of Pt-PdCuIr/C is $202.8 \text{ m}^2 \text{g}^{-1}_{\text{Pt}}$, which was 5.6 times larger than that of Pt/C catalyst. The high A_{EL} is favorable to MOR. The results indicate that a simple route of enhancing the catalytic efficiency of Pt-based catalysts is to modify the morphology.

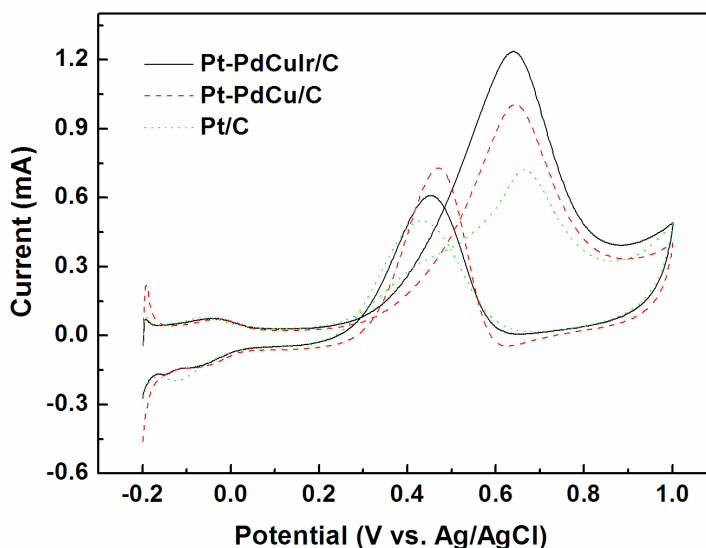


Figure 4. Cyclic voltammograms of Pt-PdCuIr/C, Pt-PdCu/C and Pt/C electrocatalysts in $0.5 \text{ mol L}^{-1} \text{CH}_3\text{OH} + 0.5 \text{ mol L}^{-1} \text{H}_2\text{SO}_4$ solution at 50 mV s^{-1} at room temperature.

The electrocatalytic activities of the Pt-PdCuIr/C electrocatalysts were evaluated for MOR. Activity of the prepared catalysts in anodic oxidation was tested in a methanol / sulfuric acid electrolyte by using CV. Fig. 4 shows CV plots of the Pt-PdCu/C, Pt/C and Pt-PdCuIr/C electrodes for MOR in $0.5 \text{ M CH}_3\text{OH}$ and $0.5 \text{ M H}_2\text{SO}_4$ at room temperature. In previous work [7], it was found that the Pt-PdCu/C electrocatalyst had superior catalytic activity to Pt/C, PtRu/C and PdCuPt/C, i.e. lower onset potential and higher oxidation current density. In this study, the result shows Pt-PdCuIr/C has a

higher catalytic activity in MOR than Pt-PdCu/C. The apparent current value of Pt-PdCuIr/C, Pt-PdCu/C and Pt/C were 1.24, 1.01, and 0.73 mA, respectively. The mass activity value of Pt-PdCuIr/C catalyst was $0.602 \text{ A mg}_{\text{Pt}}^{-1}$, which is about 6.6 times larger than that of the Pt/C catalyst ($0.091 \text{ A mg}_{\text{Pt}}^{-1}$) and about 1.2 times larger than that of Pt-PdCu/C catalyst ($0.505 \text{ A mg}_{\text{Pt}}^{-1}$), respectively.

The ratio of the forward anodic peak current (I_f) to the reverse anodic peak current (I_b) can be used to describe the CO tolerance of catalyst to accumulation of carbonaceous species [23]. A higher ratio indicates more effective removal of the poisoning species on the catalyst surface. As shown in Fig. 4, the I_f/I_b ratio of Pt-PdCuIr/C is 2.03, which was higher than those of Pt/C (1.38) and Pt-PdCu/C (1.49).

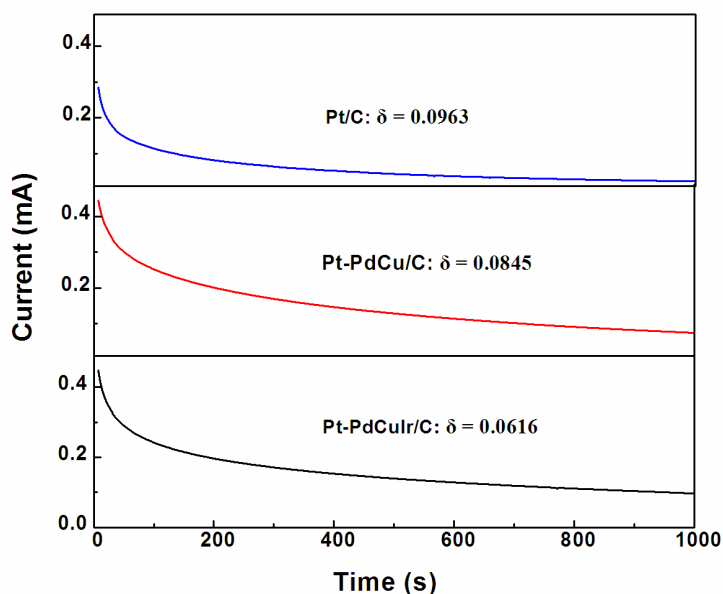


Figure 5. Chronoamperometric curves of Pt-PdCuIr/C, Pt-PdCu/C and Pt/C for methanol oxidation, polarized at a constant potential of 0.6 V vs Ag/AgCl at room temperature

Chronoamperometry tests were used to evaluate the MOR tolerance of Pt-PdCuIr/C. Fig. 5 shows the chronoamperometry curves for Pt-PdCuIr/C, Pt-PdCu/C and Pt/C electrocatalysts in 0.5 M H_2SO_4 + 0.5 M CH_3OH at a constant potential of 0.6 V (vs. Ag/AgCl) over a period of 1,000 s. The potentiostatic current initially decreased rapidly for all the electrocatalysts, which are caused by the formation of CO_{ads} and other intermediate species, such as $\text{CH}_3\text{OH}_{\text{ads}}$, CHO_{ads} and OH_{ads} , during MOR [24]. The current gradually decayed and a pseudo-steady state was achieved; this decay can be attributed to the adsorbed anion SO_4^{2-} on the surface of the catalyst, which can restrict the methanol oxidation reaction [25]. The long-term poisoning rate (δ) was calculated by measuring the linear decay of the current for a period of more than 500 s from Fig. 6 by using the following equation [25-27]:

$$\delta = \frac{100}{I_0} \times \left(\frac{dI}{dt} \right)_{t \geq 500\text{s}} \times (\% \text{s}^{-1}) \quad (2)$$

where $\left(\frac{dI}{dt}\right)_{t \geq 500s}$ is the slope of the linear portion of the current decay and I_0 is the current at the start of polarization back extrapolated from the linear current decay. The current at the Pt/C, Pt-PdCu/C and Pt-PdCuIr/C catalyst electrodes at 1000 s was 0.022, 0.074 and 0.096 mA, respectively. The calculated δ values show that the poisoning rate of the electrocatalysts followed the order of Pt-PdCuIr/C < Pt-PdCu/C < Pt/C. The lower poisoning rate of the Pt-PdCuIr/C electrocatalyst and the higher poisoning rate of Pt-PdCu/C and Pt/C catalysts exhibit the important effects of morphological structure and composition. The relatively lower poisoning rate of Pt-PdCuIr/C indicates a higher tolerance to intermediate species formed during the methanol oxidation reaction, which will be beneficial for long-term durability of DMFCs.

The activity of metal alloy catalysts in the anodic reaction has been attributed to a bifunctional effect [14]. Here, the presence of the secondary metal catalyst is thought to (i) assist Pt by oxidatively removing poisoning species from the surface and (ii) generate active oxygen species, OH_{ads} , through dissociative absorption of water. The above results exhibit that the larger surface area of the Pt-PdCuIr/C catalyst likely provides more active sites for the bifunctional mechanism.

4. CONCLUSIONS

In summary, a carbon-supported core-shell structured electrocatalyst, Pt-PdCuIr/C, for methanol oxidation was successfully prepared via a two-stage method. The structure of Pt-PdCuIr/C was investigated by XRD, TEM and electrochemical techniques. Electrochemical results of Pt-PdCuIr/C showed excellent MOR catalytic performance and its mass activity for methanol oxidation was 6.6 times higher than that of Pt/C catalyst. Pt-PdCuIr/C also showed high stability in MOR, making it an ideal candidate for the acidic environments of DMFCs applications. This work further proves that catalytic activity of Pt-based catalysts can be improved by controlling not only the size and shape of the Pt nanoparticles but also its interaction with other metal nanoparticles.

ACKNOWLEDGMENTS

We greatly appreciate the National Natural Science Foundation of China (21163018), the National Science Foundation for Post-doctoral Scientists of China (20110490847), Guangdong Key Lab for Fuel Cell Technology and the South African NRF (SFP20110918000027143) for financially supporting this work.

References

1. M.K. Debe, *Nature*, 486 (2012) 43-51.
2. A.B. Kashyout, A.A.A. Nassr, L. Giorgi, T. Maiyalagan, B.A.B. Youssef, *Int. J. Electrochem. Sci.*, 6 (2011) 379-393.
3. S. Sundarrajan, S.I. Allakhverdiev, S. Ramakrishna, *Int. J. Hydrogen Energy*, 37 (2012) 8765-8786.

4. M.M. Tusi, N.S.D. Polanco, M. Brandalise, O.V. Correa, J.C. Villalba, F.J. Anaissi, A.O. Neto, E. Spinace, *Int. J. Electrochem. Sci.*, 6 (2011) 484-491.
5. A.B. Anderson, *PCCP* 14 (2012) 1330-1338.
6. V. Mazumder, Y. Lee, S. Sun, *Adv. Funct. Mater.*, 20 (2010) 1224-1231.
7. R. Wang, Z. Zhang, H. Wang, Z. Lei, *Electrochem. Commun.*, 11 (2009) 1089-1091.
8. C.-H. Chen, L.S. Sarma, D.-Y. Wang, F.-J. Lai, C.-C. Al Andra, S.-H. Chang, D.-G. Liu, C.-C. Chen, J.-F. Lee, B.-J. Hwang, *ChemCatChem* 2(2010) 159-166.
9. H. Wang, S. Ji, W. Wang, V. Linkov, S. Pasupathi, R.F. Wang, *Int. J. Electrochem. Sci.*, 7 (2012) 3390-3398.
10. H. Wang, V. Linkov, S. Ji, W. Zhang, Z. Lei, R. Wang, *S. Afr. J. Chem.*, 65 (2012) 69-74.
11. H. Li, D.L. Kang, H. Wang, R.F. Wang, *Int. J. Electrochem. Sci.*, 6 (2011) 1058-1065.
12. S. Guo, S. Dong, E. Wang, *ACS Nano*, 4 (2009) 547-555.
13. L. Wang, Y. Nemoto, Y. Yamauchi, *J. Am. Chem. Soc.*, 133 (2011) 9674-9677.
14. H. Wang, R. Wang, H. Li, Q. Wang, J. Kang, Z. Lei, *Int. J. Hydrogen Energy*, 36 (2011) 839-848.
15. P. Holt-Hindle, Q.F. Yi, G.S. Wu, K. Koczur, A.C. Chen, *J. Electrochem. Soc.*, 155 (2008) K5-K9.
16. K.-S. Lee, S.J. Yoo, D. Ahn, T.-Y. Jeon, K.H. Choi, I.-S. Park, Y.-E. Sung, *Langmuir*, 27 (2011) 3128-3137.
17. R. Wang, H. Wang, B. Wei, W. Wang, Z. Lei, *Int. J. Hydrogen Energy*, 35 (2010) 10081-10086.
18. R.F. Wang, B.X. Wei, H. Wang, S. Ji, J. Key, X.T. Zhang, Z.Q. Lei, *Ionics*, 17 (2011) 595-601.
19. H. Wang, X. Zhang, R. Wang, S. Ji, W. Wang, Q. Wang, Z. Lei, *J. Power Sources*, 196 (2011) 8000-8003.
20. X.-B. Zhang, J.-M. Yan, S. Han, H. Shioyama, Q. Xu, *J. Am. Chem. Soc.*, 131 (2009) 2778-2779.
21. J. Barranco, A.R. Pierna, *J. Power Sources*, 169 (2007) 71-76.
22. J. Yang, C.H. Cheng, W. Zhou, J.Y. Lee, Z. Liu, *Fuel Cells*, 10 (2010) 907-913.
23. R. Wang, H. Li, H. Feng, H. Wang, Z. Lei, *J. Power Sources*, 195 (2010) 1099-1102.
24. B. Shyam, T.M. Arruda, S. Mukerjee, D.E. Ramaker, *J. Phys. Chem. C*, 113 (2009) 19713-19721.
25. J. Jiang, A. Kucernak, *J. Electroanal. Chem.*, 533 (2002) 153-165.
26. J. Jiang, A. Kucernak, *J. Electroanal. Chem.*, 543 (2003) 187-199.
27. J.W. Guo, T.S. Zhao, J. Prabhuram, R. Chen, C.W. Wong, *Electrochim. Acta*, 51 (2005) 754-763